PNAS RESEARCH ARTICLE | DEVELOPMENTAL BIOLOGY

Positive regulation of Hedgehog signaling via phosphorylation of GLI2/GLI3 by DYRK2 kinase

Saishu Yoshida[a,1,2], Akira Kawamura[a], Katsuhiko Aoki[b], Pattama Wiriyasermkul[c,d], Shinya Sugimoto[e,f,g], Junnosuke Tomiyoshi[a], Ayasa Tajima[c,h], Yamato Ishida[i], Yohei Katoh[i,3], Takehiro Tsukada[j], Yousuke Tsuneoka[k], Kohji Yamada[a], Shushi Nagamori[c,d], Kazuhisa Nakayama[i], and Kiyotsugu Yoshida[a,1]

Affiliations are included on p. 10.

Edited by Frederic de Sauvage, Genentech Inc., South San Francisco, CA; received November 16, 2023; accepted June 2, 2024

Hedgehog (Hh) signaling, an evolutionarily conserved pathway, plays an essential role in development and tumorigenesis, making it a promising drug target. Multiple negative regulators are known to govern Hh signaling; however, how activated Smoothened (SMO) participates in the activation of downstream GLI2 and GLI3 remains unclear. Herein, we identified the ciliary kinase DYRK2 as a positive regulator of the GLI2 and GLI3 transcription factors for Hh signaling. Transcriptome and interactome analyses demonstrated that DYRK2 phosphorylates GLI2 and GLI3 on evolutionarily conserved serine residues at the ciliary base, in response to activation of the Hh pathway. This phosphorylation induces the dissociation of GLI2/GLI3 from suppressor, SUFU, and their translocation into the nucleus. Loss of *Dyrk2* in mice causes skeletal malformation, but neural tube development remains normal. Notably, DYRK2-mediated phosphorylation orchestrates limb development by controlling cell proliferation. Taken together, the ciliary kinase DYRK2 governs the activation of Hh signaling through the regulation of two processes: phosphorylation of GLI2 and GLI3 downstream of SMO and cilia formation. Thus, our findings of a unique regulatory mechanism of Hh signaling expand understanding of the control of Hh-associated diseases.

Hedgehog signaling | DYRK2 | GLI2 and GLI3 | primary cilia

Significance

Hedgehog (Hh) signaling is critical for development and tumorigenesis. However, the mechanism that activates GLI2 and GLI3 following Smoothened (SMO) activation is a major unresolved question in Hh signaling. Here, we identify the ciliary kinase DYRK2 as a "positive" regulator of GLI2 and GLI3 in skeletal development but not in neural tube development. Strictly dependent on SMO activation, DYRK2 phosphorylates the evolutionarily conserved sites, $GLI2^{S252}$ and $GLI3^{S313}$ to dissociate the suppressor of fused (SUFU) from GLI2 and GLI3, resulting in activation of Hh signaling. These findings illuminate the mechanisms filling a critical gap in the activation of Hh signaling and lead to an understanding of the tissue-specific regulation of cilium-generated signaling and development of treatments for Hh-associated diseases.

Hedgehog (Hh) signaling is an evolutionarily conserved signaling pathway that plays a crucial role in embryogenesis and tumorigenesis (1–4). Upon the binding of ligands (sonic Hedgehog (SHH), indian hedgehog (IHH), and desert hedgehog (DHH)) to Patched1 (PTCH1), the essential transcription factors GLI2 and GLI3 are activated to induce the expression of *Gli1*, a master amplifier of Hh signaling (5). GLI1, GLI2, and GLI3 regulate the expression of specific and redundant target genes that are involved in cell proliferation, survival, and stemness (6, 7). Unlike other core developmental signaling pathways, vertebrate Hh signaling is uniquely and completely dependent on primary cilia, which are microtubule-based organelles protruding from the cell surface (8). Within primary cilia, the trafficking of Hh components is mediated by the intraflagellar transport machinery (9, 10). Therefore, the dysfunction and morphological abnormality of cilia, caused by defects in intraflagellar transport, affect embryonic development and adult homeostasis, resulting in a variety of human diseases, collectively referred to as ciliopathies (11).

Hh signaling is known to be an inhibitory regulation system controlled by the master negative regulator, protein kinase A (PKA) (12–14). In the "Hh signaling OFF" state, namely, in the absence of a Hh ligand, PTCH1 and GPR161 (a G protein-coupled receptor (GPCR) that is coupled to Gs) are localized on the ciliary membrane (15). GPR161 triggers the cyclic adenosine monophosphate (cAMP)-dependent PKA-mediated phosphorylation of GLI2 and GLI3 at specific serine residues (S849, S865, S877, S907, S980, and S1006 in human GLI3; i.e., PKA sites P1–6) (16–18). This phosphorylation induces further phosphorylation by GSK3β, facilitating the interaction of GLI3 with βTrCP, resulting in the generation of the N-terminal repressor form, $GLI3^{Rep}$ (19). Another negative regulator, SUFU, inhibits Hh signaling by retaining GLI2 and GLI3 in the cytoplasm and blocking their nuclear translocation. Consequently, the loss of SUFU results in the maximal activation of Hh signaling, independently of the Hh ligand and primary cilia (20–23).

In the "Hh signaling ON" state, the binding of Hh ligands to PTCH1 initiates the activation and translocation into primary cilia of the class F GPCR Smoothened (SMO), concurrently triggering the removal of GPR161 from cilia (24). This leads to a decrease in PKA activity, and subsequently a reduction in the phosphorylation levels of GLI2 and GLI3 at the PKA

The authors declare no competing interest.

This article is a PNAS Direct Submission.

[1]To whom correspondence may be addressed. Email: saishu.yoshida@sci.toho-u.ac.jp, or kyoshida@jikei.ac.jp.

[2]Present address: Department of Biomolecular Science, Toho University, Chiba 274-8510, Japan.

[3]Present address: Hiroshima University Genome Editing Innovation Center, Higashi-Hiroshima, Hiroshima 739-0046, Japan.

This article contains supporting information online at https://www.pnas.org/lookup/suppl/doi:10.1073/pnas.2320070121/-/DCSupplemental.

Published July 5, 2024.

sites (15). Furthermore, upon Hh pathway stimulation, GLI2 and GLI3 complexed with SUFU are rapidly recruited to primary cilia, followed by rapid complex disassembly, resulting in the translocation of their active forms, $GLI2^{A}$ and $GLI3^{A}$, into the nucleus (17, 25).

Notably, prevention of $GLI3^{Rep}$ production by dephosphorylation of the PKA sites alone is not sufficient to fully illustrate Hh signaling activation (17, 18), suggesting the presence of a crucial unidentified component(s) linking SMO activation and $GLI2^{A}$/$GLI3^{A}$ generation in cilia. Although posttranslational modifications (PTMs) of GLI2 and GLI3 are assumed to be involved in this process (18), the mechanism following SMO activation remains to be elucidated; namely, how Hh pathway activation promotes the dissociation of GLI2/GLI3 from SUFU, their conversion into $GLI2^{A}$/$GLI3^{A}$, and their subsequent translocation into the nucleus remain key questions in Hh signaling. Clarifying the positive regulators of GLI2 and GLI3 will provide important insights into Hh signaling and may contribute to the development of innovative therapies targeting Hh-associated diseases, particularly cancer.

In the present study, we identified DYRK2 as a positive regulator of Hh signaling, which acts via its phosphorylation of GLI2 and GLI3. Using knockout and knockdown approaches, we demonstrated that DYRK2 is responsible for Hh signaling activation both in vitro and in vivo. Mechanistically, DYRK2 phosphorylates highly conserved serine residues ($GLI2^{S252}$/$GLI3^{S313}$) by a mechanism that is dependent on the activation of SMO, facilitating the dissociation of GLI2/GLI3 from SUFU, and their subsequent nuclear translocation. Thus, the ciliary kinase DYRK2 governs activation of Hh signaling through the regulation of two processes: phosphorylation of GLI2 and GLI3 downstream of SMO and cilia formation.

Results

DYRK2, a Ciliary Kinase, Interacts with GLI2 and GLI3. The activation of Hh signaling components in primary cilia (8) suggests that ciliary kinases may function as posttranslational modifiers of these components. Hence, we focused on ciliary kinases belonging to the cyclin-dependent kinase/mitogen-activated protein kinase/glycogen synthase kinase 3/CDK-like kinase (CDK/MAPK/GSK3/CLK) (CMGC) group, which are known to negatively regulate ciliary length but have uncharacterized roles in Hh signaling (*SI Appendix,* Fig. S1*A*) (26–35). First, we transiently knocked down CMGC kinases in primary mouse embryonic fibroblasts (MEFs), and then stimulated the MEFs with the SMO agonist SAG, which significantly increased *Gli1* and *Ptch1* expression in control MEFs, indicating activation of Hh signaling (*SI Appendix,* Fig. S1*B*). Consistent with previous reports, the transient knockdown of individual CMGC kinases induced the elongation of primary cilia (*SI Appendix,* Fig. S1 *C–F*), and suppressed the expression of *Gli1* and *Ptch1* to varying degrees in response to SAG stimulation (*SI Appendix,* Fig. S1 *G* and *H*). Notably, *Dyrk2* knockdown resulted in the strongest suppression of Hh signaling (*SI Appendix,* Fig. S1 *G* and *H*). Comprehensive whole-genome RNA sequencing of the MEFs demonstrated consistent reductions in the expression of Hh target genes following the transient knockdown and knockout of *Dyrk2* (Fig. 1 *A* and *B* and *SI Appendix,* Table S1). These findings suggest that DYRK2 plays an important role in the regulation of Hh signaling, as well as in ciliary length control.

Therefore, we next aimed to identify proteins that interact with DYRK2 during Hh signaling using the BioID proximity biotinylation system (36, 37). For this purpose, we selected NIH3T3 cells based on their ability to form primary cilia and their robust responsiveness to Hh ligands. We established NIH3T3 cells with a doxycycline (Dox)-inducible DYRK2-BioID2-HA fusion construct containing a modified promiscuous biotin ligase (BioID2) (*SI Appendix,* Fig. S2*A*). We confirmed the Dox-inducible expression of DYRK2, as well as its localization to the ciliary base (i.e., at γ-tubulin-positive basal bodies, and at the proximal end of the axoneme) (Fig. 1*C*), similar to that in previous analysis, which involved transient overexpression of DYRK2 using a partially truncated low-activity CMV promoter (28), and the expression of *Gli1* and *Ptch1* upon SAG treatment (*SI Appendix,* Fig. S2*B*). Proteomic analysis of biotinylated proteins that were affinity-purified with streptavidin (SAv) beads identified several candidates, including proteins previously reported to interact with DYRK2, such as UBR5, VPRBP, and KATANIN, in the EDVP complex (38), and NOTCH1 (39) (Fig. 1*D* and data deposited in Japan ProteOme Standard Repository ID: JPST002229). Reactome pathway and STRING analysis showed that candidates for DYRK2-interacting proteins were enriched in the "Signaling by Hh" term (*SI Appendix,* Fig. S2*C* and Table S2). Notably, GLI3 (Fig. 1*E* and *SI Appendix,* Fig. S2*C* and Table S2) and GLI2 (Fig. 1*E*) were pulled down with SAv beads under Dox-induced conditions.

Identification of Phosphorylation Sites on GLI2 and GLI3 by DYRK2. As BioID analysis identified GLI2 and GLI3 as unique candidates that interact directly or indirectly with DYRK2, we then investigated whether DYRK2 phosphorylates GLI2 and GLI3. To this end, we analyzed whether the transient overexpression of CMGC kinases causes electrophoretic mobility shifts in coexpressed GLI2 and GLI3. In line with the reduction of SAG responsiveness in *Dyrk2*-knockdown cells (*SI Appendix,* Fig. S1 *G* and *H*), the overexpression of DYRK2, but not that of any other kinase analyzed, induced mobility shifts in coexpressed FLAG-GLI2 or FLAG-GLI3 (Fig. 2*A* and *SI Appendix,* Fig. S3). These shifts were detected by the overexpression of wild-type DYRK2, but not by the overexpression of the DYRK2-K251R (KR) construct, which is a kinase-dead mutant (28, 40) (Fig. 2 *B* and *C*). These band shifts were eliminated by treatment with lambda protein phosphatase (Fig. 2 *D* and *E*). Furthermore, the results of coimmunoprecipitation (IP) experiments demonstrated that DYRK2 forms complexes with GLI2 and GLI3, consistent with the results from the BioID analysis (Fig. 2 *D* and *E*).

Previously, by performing an in vitro kinase assay with purified DYRK2 protein and peptide fragments of GLI2, Varjosalo et al. showed that DYRK2 phosphorylates human GLI2 at S388 and S1011, a residue that is conserved in vertebrates but not in *Drosophila* Ci and a residue that is not conserved in *Danio rerio* among vertebrates, respectively (41) (*SI Appendix,* Fig. S4). To identify the phosphorylation sites of GLI2 and GLI3 by DYRK2 in the cellular model, we investigated candidate sites that were conserved among species using the DYRK2 consensus sequence [R-x-(x)-S/T-P] (*SI Appendix,* Fig. S4) (42–44) in addition to $GLI2^{S388}$ and $GLI2^{S1011}$. The mobility shift assay, conducted with serine/alanine (S/A) or threonine/alanine (T/A) mutants of GLI2 and GLI3, demonstrated that the $GLI2^{S104A}$, $GLI2^{S252A}$, and $GLI3^{S313A}$ mutations suppress the shifts (Fig. 2 *F* and *G*). Interestingly, the amino acid sequences of $GLI2^{S252}$ and $GLI3^{S313}$ are highly conserved not only across vertebrate species, ranging from *D. rerio* to *Homo sapiens*, but also between GLI2 and GLI3 (*SI Appendix,* Fig. S5*A*).

To monitor the phosphorylation states of $GLI2^{S252}$ and $GLI3^{S313}$, we raised a phosphorylation-specific antibody, which we named anti-phos$GLI2^{S252}$/$GLI3^{S313}$ (*SI Appendix,* Fig. S5*A*). Overexpression of DYRK2 together with wild-type GLI2 or GLI3, but not with $GLI2^{S252A}$ or $GLI3^{S313A}$, resulted in a marked enhancement in the band intensity detected by the anti-phos$GLI2^{S252}$/$GLI3^{S313}$ antibody (*SI Appendix,* Fig. S5 *B* and *C*). In line with the mobility shift assay

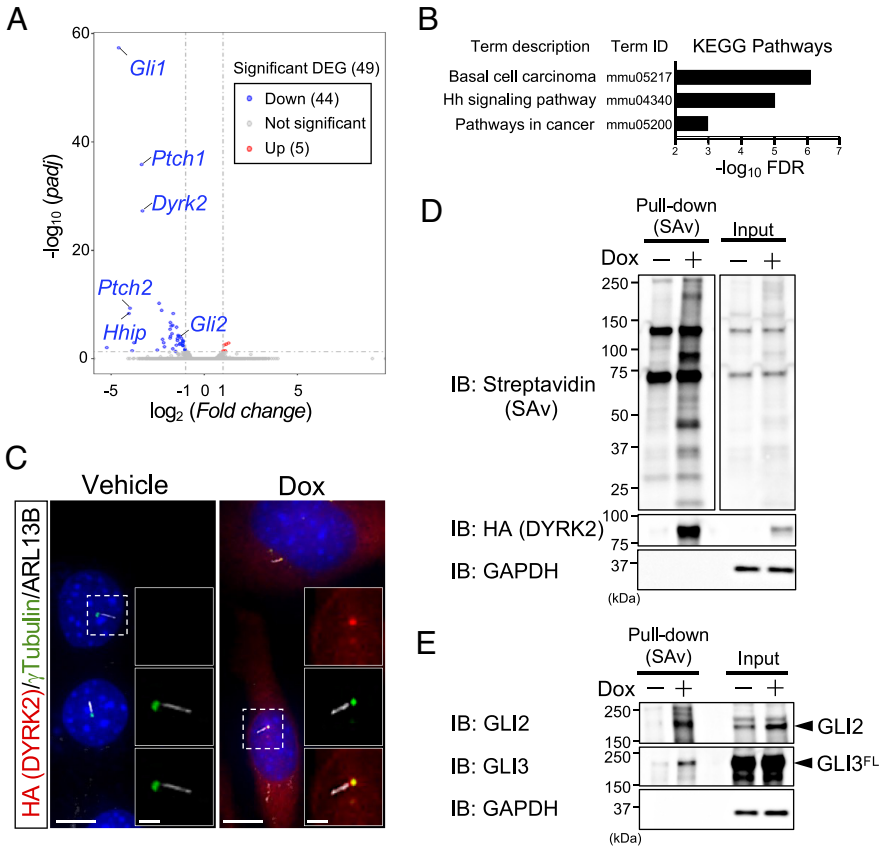

Fig. 1. DYRK2 interacts with GLI2 and GLI3. (*A* and *B*) Volcano plot representation (*A*) and KEGG pathways (*B*) of common differentially expressed genes (DEG) in transient knockdown (si*Dyrk2* versus siNegative) and knockout (*Dyrk2*$^{-/-}$ versus wild-type) MEFs. KEGG pathway analysis demonstrated that the 44 commonly down-regulated genes after knockdown and knockout of *Dyrk2* were enriched in the "Hh signaling pathway" term (Term ID: mmu04340, FDR = 1.21E-05). (*C*) Localization of DYRK2 in Dox-inducible NIH3T3 cells expressing DYRK2-BioID2-HA. Cells were cultured in the absence or presence of 1 μg/mL Dox and immunostained with antibodies against HA (red), ARL13B (white), and γ-tubulin (green). The solid line boxes on the *Right* are enlarged images of the area in the dotted line box. (Scale bar, 5 μm.) (*D* and *E*) IB of biotinylated proteins purified using SAv beads from NIH3T3 cells expressing DYRK2-BioID2-HA. The expression of DYRK2-BioID2-HA was induced by the treatment of the cells with 1 μg/mL Dox for 24 h. Cell lysates were subjected to pull-down using SAv beads. After SDS-PAGE and blotting, biotinylated proteins and DYRK2-BioID2-HA were detected with SAv and anti-HA antibody, respectively (*D*). (*E*) IB analysis of GLI2 and GLI3 in biotinylated proteins purified using SAv beads from NIH3T3 cell lysates expressing DYRK2-BioID2-HA. GAPDH was used as a loading control.

(Fig. 2*A*), the band of phosGLI2^{S252} or phosGLI3^{S313} was significantly induced by the overexpression of DYRK2, but not by that of any other CMGC kinase (Fig. 2*H*). Furthermore, an in vitro kinase assay using His tag-hGLI3$_{111\text{-}343}$ demonstrated that recombinant DYRK2 causes GLI3^{S313} phosphorylation (Fig. 2*I*). Altogether, these findings showed that DYRK2 interacts or forms complexes with GLI2 and GLI3, and specifically phosphorylates the highly conserved serine residues, GLI2^{S252} and GLI3^{S313}.

Dynamic Regulation of GLI2 and GLI3 Phosphorylation by DYRK2 at the Ciliary Base in Response to Hh Pathway Activation. As GLI2 and GLI3 are not functionally regulated by the Hh ligand when they are overexpressed (17, 18), we compared the processing and phosphorylation states of endogenous GLI2 and GLI3 in wild-type and *Dyrk2*$^{-/-}$ MEFs. Under basal conditions, full-length GLI3 proteins (GLI3^{FL}) are truncated to their N-terminal repressor forms (GLI3^{Rep}) (5). Immunoblotting (IB) analysis of GLI3 in subcellular fractions of wild-type MEFs revealed that SAG stimulation suppresses the formation of GLI3^{Rep}, resulting in a decrease in the ratio of GLI3^{Rep}/GLI3^{FL} specifically in the nuclear fraction (Fig. 3 *A* and *B*) (5). However, in *Dyrk2*$^{-/-}$ MEFs, the GLI3^{Rep} level in the nucleus remained unchanged compared with that in wild-type MEFs under SAG-stimulated conditions (Fig. 3 *A* and *B*). Considering the suppression of Hh signaling in *Dyrk2*-knockdown and -knockout cells (Fig. 1*A*), these data indicate that DYRK2 plays a crucial role in the activation of Hh signaling via suppressing GLI3^{Rep} formation.

Hence, using the anti-phosGLI2^{S252}/GLI3^{S313} antibody, we then analyzed the phosphorylation state of endogenous GLI3 immunoprecipitated with a polyclonal antibody that recognizes both GLI3^{FL} and GLI3^{Rep}. Specifically, after 3 h of SAG stimulation, GLI3^{S313} phosphorylation was significantly induced in GLI3^{FL} but not in GLI3^{Rep} (Fig. 3 *C* and *D*). More importantly, the band of phosGLI3^{S313} was absent in *Dyrk2*$^{-/-}$ MEFs (Fig. 3 *C* and *D*). Similarly, phosGLI3^{S313} was induced by SHH-N treatment for 3 h in wild-type but not *Dyrk2*$^{-/-}$ MEFs (*SI Appendix*, Fig. S6 *A* and *B*). Taken together with the findings from the overexpression analysis of CMGC kinases (Fig. 2*H*), these data show that the phosphorylation of GLI3^{FL} after the activation of SMO was induced by DYRK2.

In mammals, GLI2 and GLI3 accumulate in cilia and are assumed to be activated (GLI^{A}) at the ciliary tip upon Hh pathway stimulation (21, 25, 45, 46). In our previous study, GLI2, GLI3, and SUFU showed abnormal localization in *Dyrk2*$^{-/-}$ MEFs, whereas SMO localization remained unaffected (28). We therefore analyzed the localization of endogenous phosGLI2^{S252} and phosGLI3^{S313} as well as total GLI2 and GLI3 using immunocytostaining (Fig. 3*E*). In response to SAG stimulation, immunopositive signals for both GLI2 and GLI3 were observed at the ciliary tip (Fig. 3*E* and *SI Appendix*, Fig. S6*C*). Consistent with the results

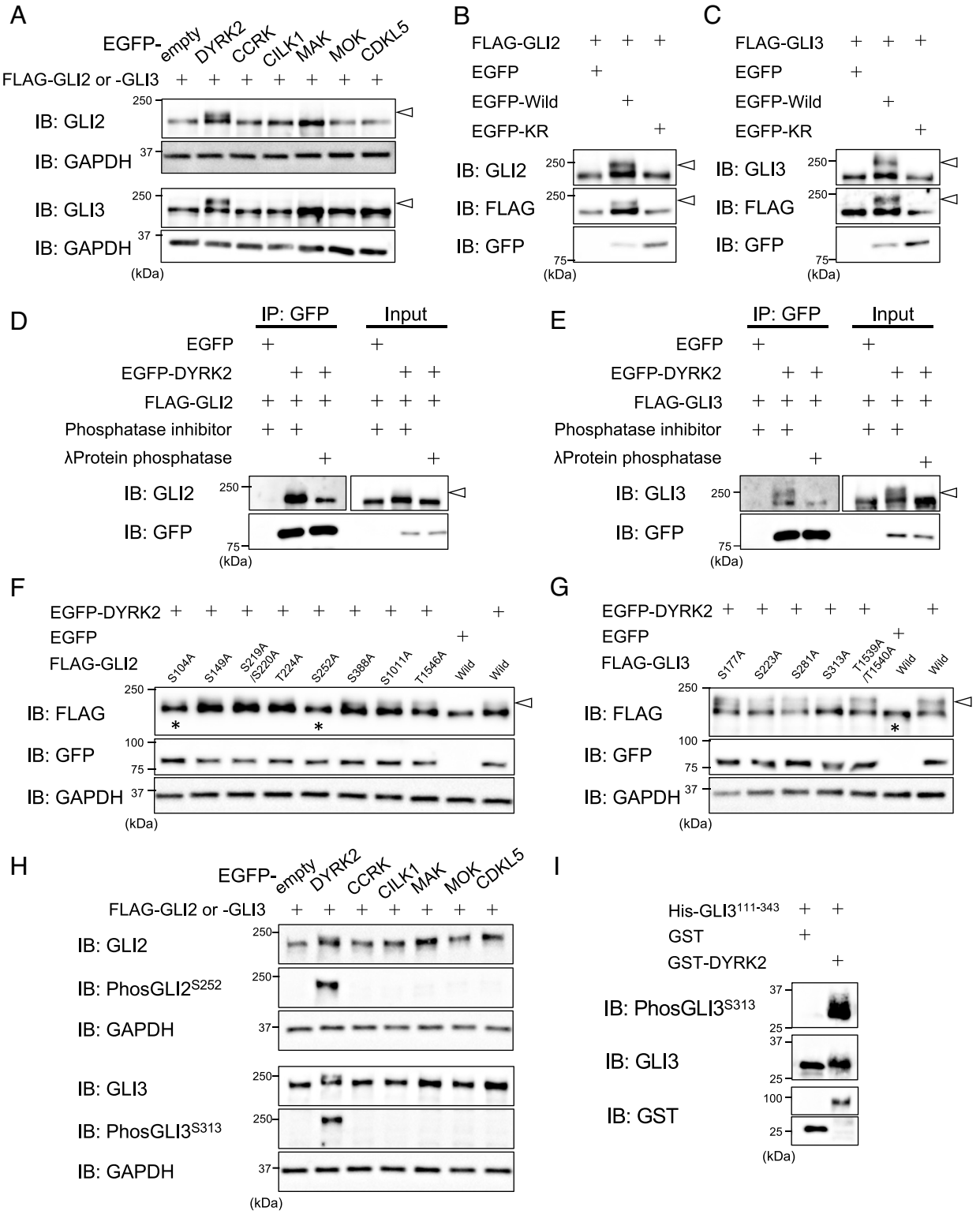

Fig. 2. Identification of phosphorylation sites for GLI2 and GLI3 by DYRK2. (*A*) Electrophoretic mobility shift of GLI2 and GLI3 induced by DYRK2 overexpression. Lysates from Lenti-X 293T cells overexpressing EGFP or EGFP-tagged CMGC kinase (DYRK2, CCRK, CILK1, MAK, MOK, or CDKL5) together with FLAG-GLI2 or FLAG-GLI3 were subjected to SDS-PAGE and IB analysis with anti-GLI2 and anti-GLI3 antibodies. (*B* and *C*) The electrophoretic mobility shift of GLI2 and GLI3 depends on DYRK2 kinase activity. Lysates from Lenti-X 293T cells overexpressing EGFP, EGFP-DYRK2 (wild-type), or EGFP-DYRK2-KR (kinase dead; K251R) together with FLAG-GLI2 (*B*) or FLAG-GLI3 (*C*) were analyzed by IB. (*D* and *E*) Effect of phosphatase treatment on the mobility of GLI2 and GLI3 following overexpression of DYRK2. Lysates from Lenti-X 293T cells overexpressing EGFP or EGFP-DYRK2 together with FLAG-GLI2 (*D*) or FLAG-GLI3 (*E*) were treated with or without lambda protein phosphatase followed by IP with anti-GFP agarose and subsequent IB. (*F* and *G*) Identification of phosphorylation sites on GLI2 and GLI3 by DYRK2 using S/A and T/A mutants. Lysates from Lenti-X293T cells overexpressing EGFP or EGFP-DYRK2 together with the FLAG-GLI2 (*F*) or FLAG-GLI3 (*G*) construct as indicated were analyzed by IB. Asterisks indicate lanes with a reduction in the mobility shift compared with the wild-type (wild) construct. In all panels, arrowheads indicate the positions of the shifted bands. (*H*) IB with the anti-phosGLI2^{S252}/GLI3^{S313} antibody. Lysates from Lenti-X 293T cells overexpressing EGFP or EGFP-tagged CMGC kinase (DYRK2, CCRK, CILK1, MAK, MOK, or CDKL5) together with FLAG-GLI2 or FLAG-GLI3 were subjected to SDS-PAGE and IB analysis with anti-GLI2, anti-GLI3, and anti-phosGLI2^{S252}/GLI3^{S313} antibodies. GAPDH was used as a loading control. (*I*) DYRK2 phosphorylates GLI3 on S313 in vitro. Recombinant GST-DYRK2 or GST was incubated with recombinant His-tagged human GLI3$_{111-343}$ and ATP. Reaction products were analyzed by IB with anti-phosGLI2^{S252}/GLI3^{S313}, anti-GLI3, and anti-GST antibodies.

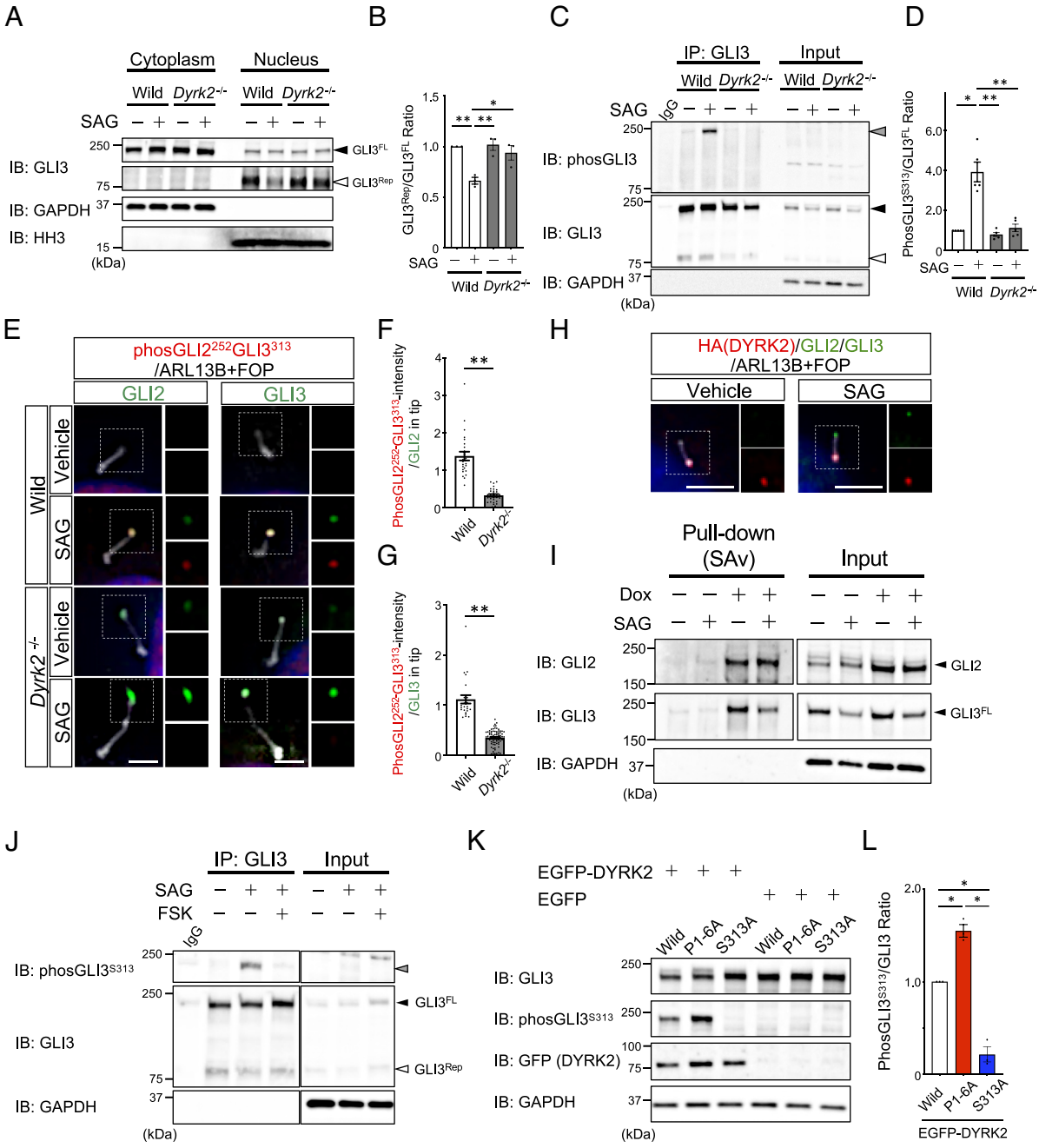

Fig. 3. Phosphorylation of GLI2 and GLI3 by DYRK2 upon SMO activation. (*A* and *B*) Protein levels of endogenous GLI3 in subcellular fractions. Nuclear and cytoplasmic fractions of wild-type and *Dyrk2*$^{-/-}$ MEFs cultured in the absence or presence of 100 nM SAG for 3 h were analyzed by IB with an anti-GLI3 antibody. GAPDH and histone H3 (HH3) are loading controls for the cytoplasmic and nuclear fractions, respectively. Closed and open arrowheads indicate the positions of GLI3^{FL} and GLI3^{Rep}, respectively. The ratio of GLI3^{Rep}/GLI3^{FL} in the nuclear fraction was calculated directly from the intensity of the individual bands in (*B*). (*C* and *D*) Phosphorylation levels of endogenous GLI3^{S313}. Lysates from wild-type and *Dyrk2*$^{-/-}$ MEFs cultured in the absence or presence of 100 nM SAG for 3 h were immunoprecipitated with an anti-GLI3 antibody followed by IB analysis using anti-phosGLI2^{S252}/GLI3^{S313} and anti-GLI3 antibodies. Gray, closed, and open arrowheads indicate the positions of phos-GLI3^{S313}, GLI3^{FL}, and GLI3^{Rep}, respectively. Ratios of phosGLI3^{S313}/GLI3^{FL} were calculated directly from the intensity of individual bands in (*D*). (*E*–*G*) Localization of phosGLI2^{S252}/GLI3^{S313} in MEFs. Wild-type and *Dyrk2*$^{-/-}$MEFs cultured in the absence or presence of 100 nM SAG for 3 h were immunostained with antibodies against phosGLI2^{S252}/GLI3^{S313} (red), ARL13B and FOP (white), and either GLI2 or GLI3 (green). Nuclei were stained with DAPI (blue). The boxes on the *Right* are single-color images of the area in the dotted line box. (Scale bar, 3 μm.) Fluorescence staining intensities of phosGLI2^{S252}/GLI3^{S313} at the ciliary tips were compared to those of GLI2 (*F*) and GLI3 (*G*). Data were pooled from three independent MEFs. Statistical significance between wild-type and *Dyrk2*$^{-/-}$ cells was determined using the Student *t* test. $^{**}P < 0.01$. (*H*) Localization of DYRK2 in Dox-inducible NIH3T3 cells expressing DYRK2-BioID2-HA. Cells cultured in the absence or presence of 200 nM SAG with 1 μg/mL Dox for 24 h were immunostained with antibodies against HA (red), GLI2 and GLI3 (green), and ARL13B and FOP (white). Nuclei were stained with DAPI (blue). The boxes on the *Right* are single-color images of the area in the dotted line box. (Scale bar, 5 μm.) (*I*) IB of biotinylated proteins purified with SAv beads from NIH3T3 cell lysates expressing DYRK2-BioID2-HA. Lysates from the cells cultured in the absence or presence of 200 nM SAG and 1 μg/mL Dox for 24 h were pulled down with SAv beads, followed by IB analysis with anti-GLI2 and anti-GLI3 antibodies. (*J*) Effect of FSK on the phosphorylation level of GLI3^{S313}. Lysates from wild-type MEFs cultured in the absence or presence of 100 nM SAG and 20 μM FSK for 3 h were immunoprecipitated using the anti-GLI3 antibody, followed by IB analysis using anti-phosGLI2^{S252}/GLI3^{S313} and anti-GLI3 antibodies. (*K* and *L*) Effect of phosphorylation site mutations on the phosphorylation level of GLI3^{S313}. Lysates from Lenti-X 293T cells overexpressing EGFP or EGFP-DYRK2 together with FLAG-GLI3 (wild-type), FLAG-GLI3 (S/A mutants at six PKA sites, P1–6A), or FLAG-GLI3^{S313A} were immunoprecipitated with an anti-FLAG antibody followed by IB using anti-GLI3 and anti-phosGLI2^{S252}/GLI3^{S313} antibodies. The ratio of phosGLI3^{S313} to total GLI3 was calculated directly from the intensity of individual bands, and the fold change was calculated by comparing the levels with that of the wild-type in (*L*). Data are presented as means ± SEM (n = 3 and 4 biological replicates, and three technical replicates per condition in *B*, *D*, and *L*, respectively). Statistical significance in *B*, *D*, and *L* was determined using one-way ANOVA, followed by the Tukey multiple comparison test. $^{*}P < 0.05$ and $^{**}P < 0.01$. In *C*, *I*, *J*, and *K*, GAPDH was used as a loading control.

of IB analysis (Fig. 3 *C* and *D*), immunopositive signals for phosGLI2^{S252}/GLI3^{S313} at the ciliary tip were significantly increased by SAG stimulation in wild-type but not *Dyrk2*$^{-/-}$ MEFs (Fig. 3 *E*–*G* and *SI Appendix,* Fig. S6*C*). Taken altogether, we conclude that the phosphorylation of GLI2^{S252} and GLI3^{S313} is triggered by DYRK2 upon the activation of SMO, and is an essential event for Hh pathway activation.

We further investigated the mechanism underlying the DYRK2-dependent phosphorylation of GLI2 and GLI3 in the Hh signaling pathway. The ciliary tip has been repeatedly proposed as a site for the activation of GLI2 and GLI3 (21, 25, 45, 46). To identify the subcellular site of DYRK2-mediated phosphorylation, we investigated the localization of DYRK2 using Dox-inducible NIH3T3 cells expressing DYRK2-BioID2-HA. Despite the repositioning of GLI2 and GLI3 to the ciliary tip in response to SAG treatment, there was no obvious difference in the localization of DYRK2-BioID2-HA between the absence and presence of SAG treatment; it was predominantly found at the ciliary base in both conditions (Fig. 3*H*). In line with the unchanged DYRK2 localization, pull-down of the cell lysates with SAv beads demonstrated that DYRK2-BioID2-HA interacts with GLI2 and GLI3 independently of SAG treatment (Fig. 3*I*). These findings show that DYRK2 has the potential to interact with GLI2 and GLI3 at the ciliary base, rather than at the ciliary tip, irrespective of Hh pathway stimulation.

We then focused on the phosphorylation substrates GLI2 and GLI3, which have been reported to undergo strict negative regulation by proteasome-mediated degradation downstream of the GPR161–cAMP–PKA axis (15). Under basal conditions, GPR161 induces PKA activation, leading to the phosphorylation of GLI3 at six distinct PKA sites (*SI Appendix,* Fig. S7*A*). Upon treatment with SAG, GPR161 is removed from cilia, resulting in a reduction in the cAMP level and PKA activity (*SI Appendix,* Fig. S7*B*). To verify the effect of PKA on DYRK2-mediated phosphorylation, we subjected lysates of cells treated with forskolin (FSK), an activator of adenylyl cyclase (*SI Appendix,* Fig. S7*C*), to IP with an anti-GLI3 antibody followed by IB with the anti-phosGLI2^{S252}/GLI3^{S313} antibody. Intriguingly, FSK abolished the phosphorylation of GLI3^{S313} upon SAG treatment (Fig. 3*J*). Based on these findings, we then investigated whether the phosphorylation of PKA sites in GLI2 and GLI3 affects their DYRK2-mediated phosphorylation. The levels of phosphorylation at GLI2^{S252} and GLI3^{S313} were significantly increased in the S/A-mutants of six PKA sites (P1–6A) compared with those in wild-type GLI2 and GLI3 (Fig. 3 *K* and *L* and *SI Appendix,* Fig. S7 *F* and *G*). On the other hand, knockout of *Gpr161* (*SI Appendix,* Figs. S8 *A* and *B* and S9 *A* and *B*), which reduces PKA activity, or treatment of cells with a PKA inhibitor (H-89) (*SI Appendix,* Fig. S8 *C*–*E*) did not induce DYRK2-mediated phosphorylation on GLI3^{S313}. Therefore, although dephosphorylation of the PKA sites enhances the efficiency of phosphorylation by DYRK2, inactivation of PKA is neither a prerequisite nor a sufficient condition for DYRK2-mediated phosphorylation. These results together suggest that the activation of GLI2 and GLI3 in the Hh signaling pathway occurs in a stepwise manner, as follows: i) decreased phosphorylation of PKA sites owing to inactivation of the GPR161–cAMP–PKA axis; ii) upon SMO activation, DYRK2-mediated phosphorylation of GLI2^{S252} and GLI3^{S313} at the ciliary base but not at the tip; and iii) transport of phosphorylated GLI2 and GLI3 to the ciliary tip.

DYRK2-Dependent Phosphorylation of GLI2 and GLI3 Triggers Their Dissociation from SUFU and Translocation into the Nucleus. In response to SAG stimulation, the GLI2/GLI3–SUFU complex enters the cilia, and the components rapidly dissociate from each other, enabling GLI2^{A} and GLI3^{A} to translocate into the nucleus (17, 25). However, the mechanism by which SAG stimulation triggers GLI2/GLI3 dissociation from SUFU, and their conversion to GLI2^{A}/GLI3^{A} remains unclear. Previous crystallographic studies have identified that the "SYGHLS" motif in GLI proteins is crucial for SUFU binding (47, 48). Interestingly, the DYRK2-mediated phosphorylation sites GLI2^{S252} and GLI3^{S313} are included in the SUFU-binding region and in proximity to SYGHLS (Fig. 4 *A* and *B*). These data suggest that DYRK2-mediated phosphorylation of GLI2 and GLI3 facilitates SUFU dissociation.

To address this possibility, we compared the interaction between endogenous GLI3 and SUFU in wild-type and *Dyrk2*$^{-/-}$MEFs under basal and SAG-stimulated conditions. As previously reported (17, 25), the level of SUFU coimmunoprecipitated with GLI3 in wild-type MEFs was substantially decreased by SAG treatment, inversely to the increase in the phosGLI3^{S313} level (Fig. 4 *C* and *D*). By contrast, SAG treatment did not change the level of coimmunoprecipitated SUFU in *Dyrk2*$^{-/-}$MEFs (Fig. 4 *C* and *D*). To further investigate whether the DYRK2-dependent phosphorylation sites (GLI2^{S252} and GLI3^{S313}) are directly involved in their interaction with SUFU, we assessed the binding strength of a nonphosphorylated (GLI3$_{309–345}$) peptide and a GLI3^{S313}-phosphorylated peptide (phospho-GLI3$^{S313}_{309–345}$) to SUFU by surface plasmon resonance (SPR) analysis (Fig. 4*E*). Consistent with a prior study (48), SUFU bound to GLI3$_{309–345}$ with a dissociation constant (K_D) of 2.64 × 10^{-6} M (Fig. 4*E*). In contrast, the phospho-GLI3$^{S313}_{309–345}$ peptide demonstrated reduced binding to SUFU, with a K_D of 5.08 × 10^{-6}M (Fig. 4*E*). Furthermore, a phosphomimetic mutant (GLI2^{S252E}) demonstrated distinct nuclear localization in contrast to the predominant cytoplasmic distribution of wild-type GLI2 and the alanine mutant (GLI2^{S252A}) (Fig. 4 *F* and *G*). Consistently, overexpression of GLI2^{S252E} significantly induced the expression of *Gli1* and *Ptch1* compared to the wild-type GLI2 or GLI2^{S252A} (Fig. 4*H*). Additionally, the efficient activation of Hh signaling by overexpression of GLI2^{S252E} was also observed in *Ift80*$^{-/-}$ and *Ift52*$^{-/-}$ primary cilia-deficient cells, as well as in *Dyrk2*$^{-/-}$ cells that exhibit morphological abnormalities of primary cilia (*SI Appendix,* Figs. S9 *C* and *D* and S10).

Considering the action of DYRK2-mediated phosphorylation of GLI2 and GLI3 upstream of SUFU, we examined the effect of *Dyrk2* knockdown on the activation of Hh signaling in *Sufu*$^{-/-}$cells (Fig. 4*I* and *SI Appendix,* Fig. S11). *Sufu*$^{-/-}$cells exhibited extremely high levels of *Gli1* expression even in the absence of SAG treatment as previously reported (*SI Appendix,* Fig. S11*B*) (20–23). The knockdown of *Dyrk2* resulted in a significant reduction with induced *Gli1* expression in wild-type, but not *Sufu*$^{-/-}$cells (Fig. 4*I* and *SI Appendix,* Fig. S11*C*). Overall, these results indicate that the DYRK2-dependent phosphorylation of GLI2 and GLI3 facilitates their dissociation from SUFU and their subsequent nuclear translocation at a step downstream of SMO, resulting in the activation of Hh signaling.

DYRK2-Mediated Phosphorylation of GLI2 Promotes Limb Development via Proliferation. We further investigated the potential role of DYRK2-mediated phosphorylation of GLI2 and GLI3 in tissue development. Analysis of *Dyrk2*$^{-/-}$ mice at embryonic day (E)18.5 and E16.5 demonstrated abnormalities in limb development, such as a noticeable reduction in bone length and ossification (Fig. 5 *A*–*E*), while neural tube development remained normal (28). In situ hybridization chain reaction (HCR) utilizing fluorophore-conjugated short hairpin DNAs (49–51) revealed that *Dyrk2* mRNA was localized in the limb buds as well as the neural tube at E10.5 (*SI Appendix,* Fig. S12). Consistent with the results of analysis using MEFs, the expression of *Gli1*

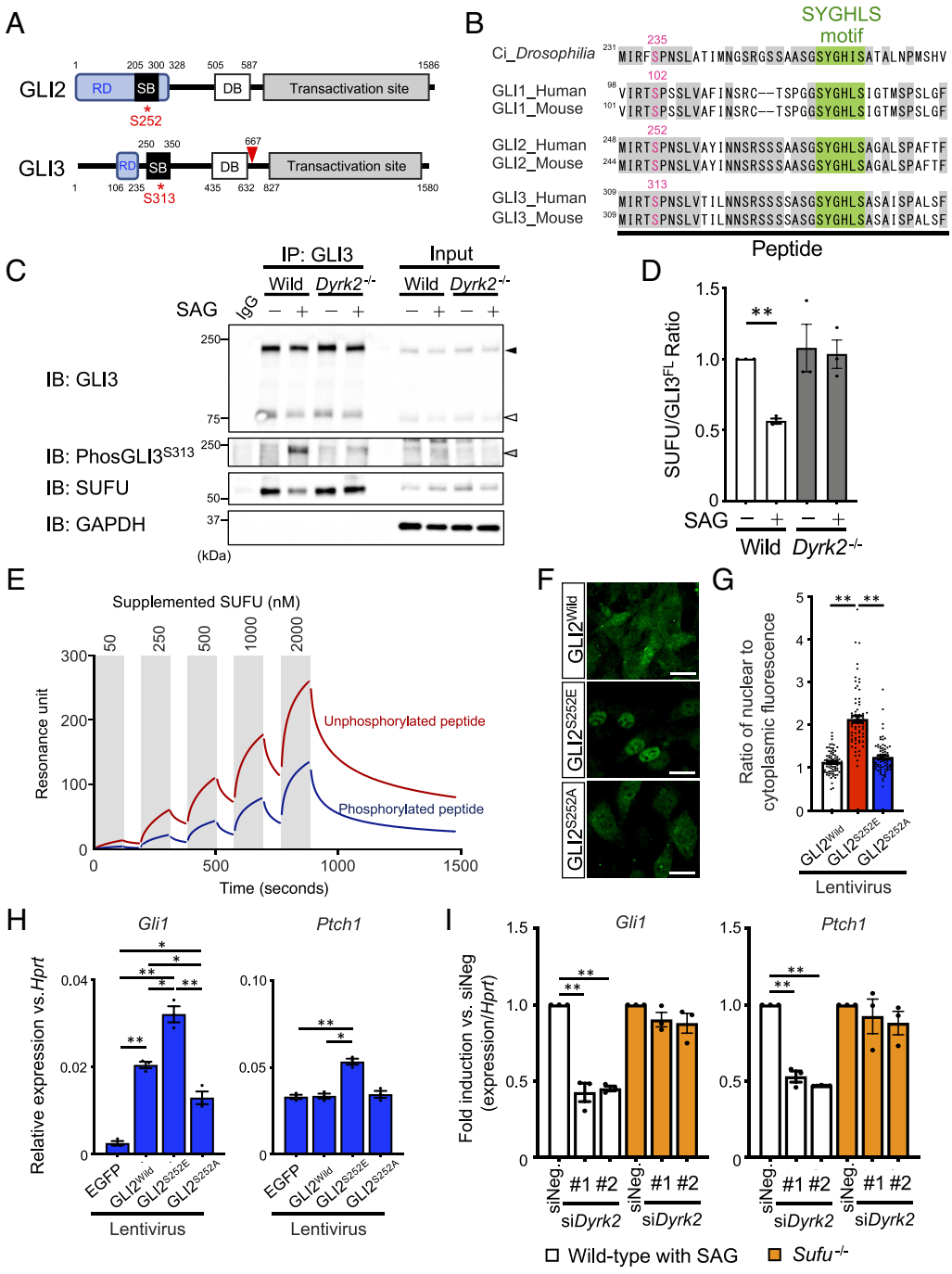

Fig. 4. Phosphorylation of GLI2 and GLI3 by DYRK2 promotes their dissociation from SUFU and their nuclear translocation. (*A*) Schematic representation of the domain organization of human GLI2 and GLI3. RD, repressor domain; SB, SUFU-binding region; DB, DNA-binding domain. The red arrowhead in GLI3 indicates the cleavage site to generate $GLI3^{rep}$. (*B*) Sequence alignment of the SB in *Drosophila* Ci, and human and mouse GLI1, GLI2, and GLI3. The phosphorylation sites by DYRK2 (human $GLI2^{S252}$ and $GLI3^{S313}$) are indicated in magenta. The SUFU binding "SYGHLS" motif and conserved amino acids between GLI2 and GLI3 are highlighted in green and gray, respectively. (*C* and *D*) Interaction of endogenous GLI3 with SUFU. Lysates from wild-type and *Dyrk2*$^{-/-}$ MEFs cultured in the absence or presence of 100 nM SAG for 3 h were immunoprecipitated with an anti-GLI3 antibody, followed by IB analysis using anti-GLI3, anti-phosGLI2^{S252}/GLI3^{S313}, and anti-SUFU antibodies. GAPDH was used as a loading control. The ratio of SUFU to $GLI3^{FL}$ in the IP fraction was calculated directly from the intensity of individual bands, and the fold change was calculated by comparing the levels relative to those of wild-type cultured in the absence of SAG in (*D*). Data are presented as means ± SEM ($n = 3$ biological replicates per condition). (*E*) SPR analysis of the binding strength of the GLI3 peptide to SUFU. SPR single-cycle analysis was performed using the nonphosphorylated GLI3 peptide ($GLI3_{309–345}$) and phosphorylated GLI3 peptide (phospho-$GLI3^{S313}{}_{309–345}$) and specific concentrations of recombinant SUFU as analytes. Analytes were loaded during the periods shaded in gray. The dissociation constant (K_D) was calculated by curve fitting for the interaction between SUFU and $GLI3_{309–345}$ with a 2:1 binding mode. (*F* and *G*) Localization analysis of GLI2 mutants. NIH3T3 cells infected with a lentiviral vector for wild-type or the indicated GLI2 construct were immunostained with antibodies against anti-GLI2. (Scale bar, 5 μm.) Quantification of the ratio of nuclear to cytoplasmic fluorescence is shown in (*G*). Data are presented as pooled from three independent experiments and as means ± SEM ($n = 3$ technical replicates per condition; >20 cells were scored for each experiment). (*H*) Effects of GLI2 expression on the activation of Hh signaling in NIH3T3 cells. NIH3T3 cells infected with a lentiviral vector for wild-type or the indicated GLI2 construct were subjected to RT-qPCR analysis for expression of *Gli1* and *Ptch1* 3 d after infection. Data are shown as the relative expression to *Hprt* and presented as means ± SEM ($n = 3$ technical replicates per condition). (*I*) Effects of knockdown of *Dyrk2* on activation of Hh signaling in *Sufu*$^{-/-}$ cells. Expression levels of *Gli1* and *Ptch1* in wild-type and *Sufu*$^{-/-}$ NIH3T3 cells cultured in the presence or absence of 100 nM SAG, respectively, and treated with two independent siRNAs for *Dyrk2* were measured by RT-qPCR. *Hprt* was used as an internal standard, and the fold change was calculated by comparing the expression levels relative to those of siNeg. Data are presented as means ± SEM ($n = 3$ technical replicates per condition). Statistical significance for each siNeg was determined by one-way ANOVA followed by the Tukey multiple comparison test. *$P < 0.05$ and **$P < 0.01$.

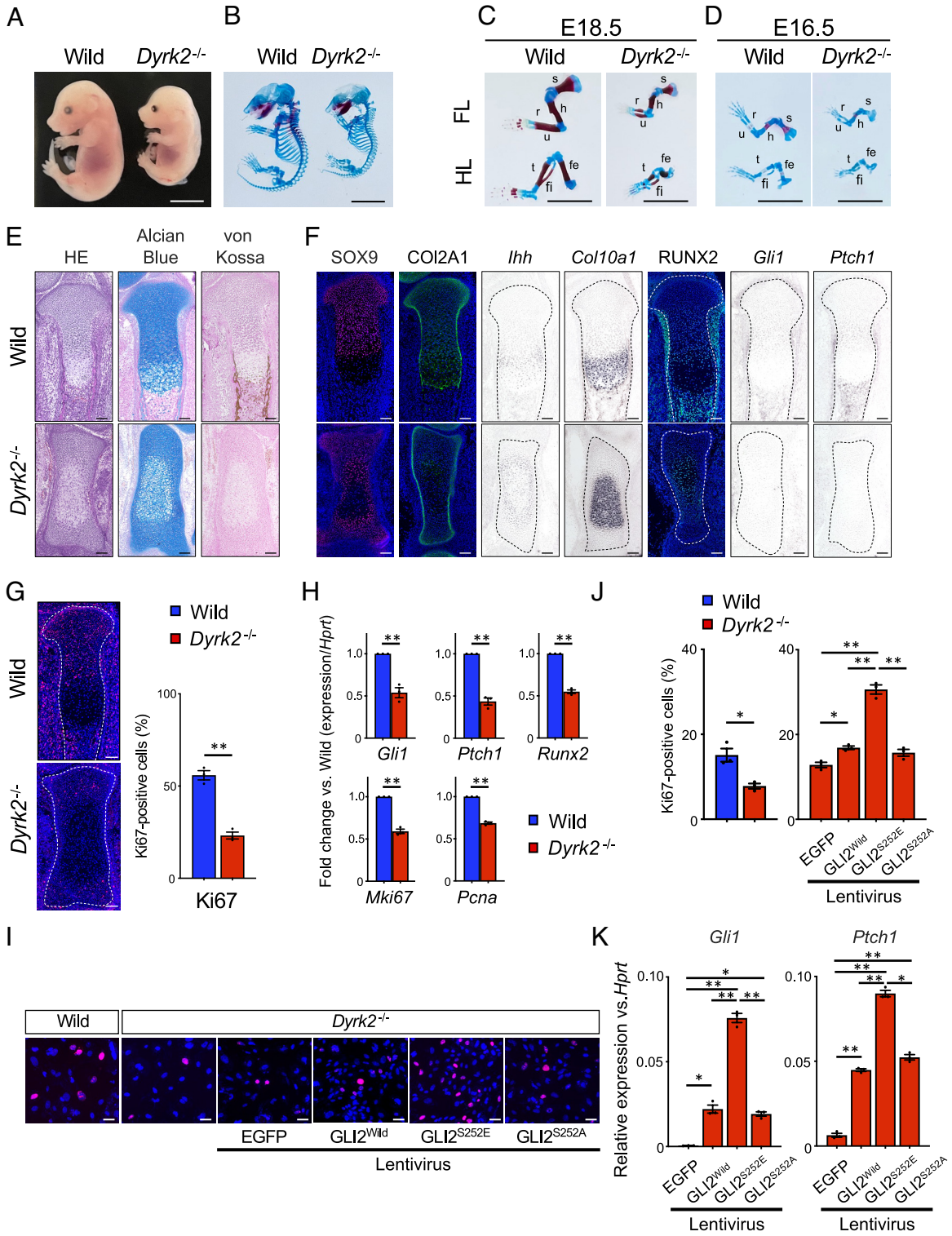

Fig. 5. DYRK2-triggered phosphorylation of GLI2 promotes limb development via proliferation. (*A*–*D*) Skeletal development in wild-type and *Dyrk2*$^{-/-}$ embryos. Gross images (*A*) and Alizarin Red and Alcian Blue staining (*B*) of whole embryos at E16.5 and forelimbs (FL) and hind limbs (HL) from embryos at E18.5 (*C*) and E16.5 (*D*) are shown. Fe, femur; fi, fibula; h, humerus; r, radius; s, scapula; t, tibia; u, ulna. (*E* and *F*) Analysis of chondrogenic differentiation in developing tibias of wild-type and *Dyrk2*$^{-/-}$ embryos at E16.5. Hematoxylin and eosin (HE), Alcian Blue, and von Kossa (calcium) staining in (*E*); and immunohistochemistry of SOX9, COL2A1, and RUNX2; and in situ hybridization of *Ihh*, *Col10a1*, *Gli1*, and *Ptch1* in (*F*). (*G*) Immunohistochemical analysis of proliferation in the periarticular and columnar proliferating regions of the tibia of wild-type and *Dyrk2*$^{-/-}$ embryos at E16.5. Measurement of the proportions of Ki67-positive cells. (*H*) RT-qPCR analysis of *Gli1*, *Ptch1*, *Runx2*, *Mki67*, and *Pcna* in the limb bud tissues from wild-type and *Dyrk2*$^{-/-}$ embryos at E11.5. *Hprt* was used as an internal standard for RT-qPCR, and the fold changes were calculated by comparing the expression levels relative to those of wild-type. (*I* and *J*) Effect of GLI2 expression on the proliferative potential of limb bud mesenchymal cells. Limb bud mesenchymal cells prepared from wild-type and *Dyrk2*$^{-/-}$ embryos at E11.5 were infected with a lentiviral vector encoding EGFP or the indicated GLI2 construct and immunostained with a Ki67 antibody (red). Nuclei were stained with DAPI (blue). Measurement of the proportions of Ki67-positive cells in wild-type and *Dyrk2*$^{-/-}$ limb bud mesenchymal cells 4 d after infection in (*J*). (*K*) Effects of DYRK2-mediated phosphorylation of GLI2^{S252} on the activation of Hh signaling. Limb bud mesenchymal cells prepared from *Dyrk2*$^{-/-}$ embryos at E11.5 were infected with a lentiviral vector encoding EGFP or the indicated GLI2 construct and subjected to RT-qPCR analysis for expression of *Gli1* and *Ptch1* 3 d after infection. Data are presented as means ± SEM (n = 3 biological replicates in *G*, *H*, *J*, and *K*). Statistical significance was determined by the Student t test in *G*, *H*, and *J* for wild-type and *Dyrk2*$^{-/-}$ and one-way ANOVA followed by the Tukey multiple comparison test in *J* and *K*. *P < 0.05 and **P < 0.01. Scale bar: 5 mm (*A*–*D*), 100 μm (*E*–*H*), and 50 μm (*J*).

and *Ptch1* was decreased in *Dyrk2*$^{-/-}$ mice compared with wild-type mice, whereas *Ihh* expression remained unaffected (Fig. 5*F*). Additionally, immunostaining for the chondrocyte marker COL2A1 and the osteoblast precursor marker RUNX2, a target gene of Hh signaling in the perichondrial region demonstrated that their signals were decreased in *Dyrk2*$^{-/-}$ embryos (Fig. 5*F*). Because limb formation involves endochondral ossification, defects in cartilage differentiation and proliferation lead to bone shortening (52, 53). Hence, we conducted an in vitro chondrogenic differentiation assay using limb bud mesenchymal cells from *Dyrk2*$^{-/-}$ embryos at E11.5. Unexpectedly, *Dyrk2*$^{-/-}$ cells differentiated into Alcian Blue-positive chondrocytes, similar to wild-type cells, in vitro (*SI Appendix,* Fig. S13*A*). We subsequently focused on assessing the proliferative capacity of *Dyrk2*$^{-/-}$ cells. Immunohistochemical analysis of the developing tibiae from *Dyrk2*$^{-/-}$ embryos at E16.5 demonstrated a significant decrease in the population of cells positive for the proliferation markers Ki67 and phospho-histone H3 (PHH3) (Fig. 5*G* and *SI Appendix,* Fig. S13*B*). Reverse transcription-qPCR (RT-qPCR) analysis showed a significant decrease in the expression of proliferation-associated genes (*Mki67* and *Pcna*) (Fig. 5*G* and *SI Appendix,* Fig. S13*B*), as well as *Gli1* and *Ptch1*, in the limb buds of *Dyrk2*$^{-/-}$ embryos at E11.5 (Fig. 5*H*). To clarify the involvement of DYRK2-mediated phosphorylation in this phenotype, we cultured primary E11.5 limb bud mesenchymal cells and found that the proportion of Ki67-positive cells was decreased in *Dyrk2*$^{-/-}$ mesenchymal cells (Fig. 5 *I* and *J*). Infection of *Dyrk2*$^{-/-}$cells with a lentivirus vector for a phosphomimetic GLI2^{S252E} mutant but not an alanine mutant (GLI2^{S252A}) caused markedly increased proliferation compared with that for wild-type GLI2 (Fig. 5 *I* and *J*). Importantly, the expression of *Gli1* and *Ptch1* was significantly induced by GLI2^{S252E} compared to the wild-type GLI2 or GLI2^{S252A} (Fig. 5*K*). Collectively, these data indicate that DYRK2-mediated phosphorylation of GLI2^{S252} contributes to limb bud development through the increased proliferation of limb bud mesenchymal cells and chondrocytes.

Discussion

The conventional understanding of Hh signaling regulation via GLI2 and GLI3 is that the inhibitory regulation system is orchestrated by the negative regulators PKA and SUFU. However, the mechanisms controlling the activation of Hh signaling downstream of SMO remain unclear, i.e., the processes by which activated SMO triggers the dissociation of GLI2/GLI3 from SUFU, their conversion into GLI2^{A}/GLI3^{A}, and their subsequent translocation into the nucleus. This intriguing and unidentified mechanism led us to speculate the potential presence of a positive posttranslational modifier for GLI2 and GLI3, distinct from the conventional negative regulator PKA. In this study, we identified DYRK2 as the kinase responsible for the activation of GLI2 and GLI3, in addition to regulating ciliary length. Loss of *Dyrk2* in mice causes skeletal malformation, but neural tube development remains normal. DYRK2-mediated phosphorylation of highly conserved serine residues of GLI2 and GLI3 (GLI2^{S252} and GLI3^{S313}) was strictly triggered in a SMO activation-dependent manner, facilitating their dissociation from SUFU and their subsequent nuclear translocation, as illustrated in *SI Appendix,* Fig. S14.

DYRK2 Is a Positive Regulator of Hh Signaling upon SMO Activation. A major unsolved issue in Hh signaling is how activated SMO participates in the activation of downstream GLI2 and GLI3. Whereas a few kinases, including ULK3 (54) and MRCKα/β (55), have been proposed as candidates for GLI2 activation, their in vivo roles remain elusive owing to a lack of comprehensive animal knockout or endogenous-level studies. Our findings demonstrated a robust increase in the phosphorylation of GLI2^{S252} and GLI3^{S313} by DYRK2 following SMO activation. Interestingly, the phosphorylation site of human GLI2^{S252} corresponds to that of mouse GLI2^{S248}, which may be a potential phosphorylation site in response to SAG stimulation, according to mass spectrometry-based selected reaction monitoring assays (18). Considering that the efficiency of phosphorylation by DYRK2 was improved by dephosphorylating the PKA sites of GLI2 and GLI3 (Fig. 3 *K* and *L* and *SI Appendix,* Fig. S7 *F* and *G*), our findings demonstrate that the mechanism that activates GLI2 and GLI3 downstream of SMO is a stepwise process, i.e., the activation of GLI2^{A}/GLI3^{A} by the positive regulator DYRK2 following inactivation of the negative regulator PKA. Taken together with the observed inhibition of *Gli1* and *Ptch1* expression in *Dyrk2*$^{-/-}$ embryos and MEFs, we conclude that DYRK2 is a positive regulator of Hh signaling through Hh component modification. Although the dephosphorylation of the PKA sites enhances the efficiency of DYRK2-mediated phosphorylation of GLI2 and GLI3, analysis using *Gpr161*$^{-/-}$ cells or the PKA inhibitor revealed that the inactivation of PKA is not prerequisite or sufficient for phosphorylation by DYRK2. How DYRK2-mediated phosphorylation is induced downstream of SMO as well as how DYRK2 is recruited to the ciliary base is an important issue to be addressed in the future.

Another question is where the active modifications of GLI2 and GLI3 occur. The ciliary tip is often considered to be the site of such modifications (21, 25, 45, 46). Humke et al. found that the conversion to GLIs^{FL} and their nuclear translocation were inhibited in *Kif3a*$^{-/-}$ mice, suggesting the importance of intraflagellar transport in the activation of GLI2 and GLI3 (25). However, DYRK2 was located at the ciliary base regardless of SAG treatment (Fig. 3 *H* and *I*), implying that DYRK2 initiates active modifications of GLI2 and GLI3 at the ciliary base rather than at the tip. Additionally, inhibitory kinases, such as PKA (14), GSK3β (56), and CK1 (57), are localized to the ciliary base. Hence, we postulate that the ciliary base acts as the site responsible for the early phosphorylation of GLI2 and GLI3, according to the following proposed model (*SI Appendix,* Fig. S14): i) Before ciliary translocation, SMO activation induces the phosphorylation of GLI2 and GLI3 at the ciliary base by DYRK2 following inactivation of PKA; ii) GLI2 and GLI3, phosphorylated by DYRK2, enter the cilia and may undergo additional modifications; and iii) the fully activated forms of GLI2 and GLI3 migrate from the cilia to the nucleus.

Molecular Mechanisms of DYRK2-Mediated Phosphorylation of GLI2 and GLI3. The mechanism underlying the dissociation of GLI2 and GLI3 from SUFU following SMO activation remains unclear. Although PKA inactivation appears to be required for the dissociation of GLI2/GLI3 from SUFU, the dephosphorylation of PKA sites (P1–6A) in GLI2 and GLI3 is insufficient to explain this mechanism for full activation of Hh signaling (17, 18). The present data show that DYRK2-mediated phosphorylation of GLI3^{S313} drives SUFU dissociation upon SMO activation in the cellular model (Fig. 4 *C* and *D*) and through biochemical techniques (Fig. 4*E*).

Interestingly, all sites phosphorylated by PKA and GSK3β, and binding sites of βTrCP are fully conserved in mice and humans (58). Recently, biochemical analyses have shown that the phosphorylation of S102, S116, and S130 in proximity to the SUFU-binding domain of GLI1, which is primarily induced at the transcriptional level (*SI Appendix,* Fig. S1*B*), cooperatively promotes SUFU dissociation (59). Notably, among these three sites in GLI1, only GLI1^{S102},

corresponding to GLI2^{S252} and GLI3^{S313}, was conserved in *Drosophila* Ci as well as in mammalian GLI2 and GLI3 (Fig. 4*B*). Given that GLI2 and GLI3 are thought to be phosphorylated at multiple sites upon SMO activation (17, 18), it is plausible that other sites must undergo PTMs in a coordinated and sequential manner to achieve complete SUFU dissociation (*SI Appendix,* Fig. S14). Further studies are essential to identify proteins involved in the PTMs of GLI2 and GLI3 upon SMO activation, as well as to clarify the role of DYRK2 in the hierarchical phosphorylation of GLI2 and GLI3.

Roles of DYRK2-Mediated Phosphorylation of GLI2 during Development. Bone length is defined by cartilage length through the proliferation of chondrocytes and progenitor cells (52, 53). During endochondral ossification, the IHH–SMO–PTHrP axis orchestrates the proliferation and maturation of chondrocytes through a negative feedback mechanism (60). *Ihh*$^{-/-}$ mice demonstrate extremely shortened limbs owing to decreased cell proliferation and accelerated chondrocyte hypertrophy with loss of *Pthrp* expression (4). *Dyrk2*$^{-/-}$ embryos demonstrate short-limb phenotypes similar to those of *Gli2*$^{-/-}$ mice (6) and chondrocyte-specific *Smo*$^{-/-}$ mice (61). The significance of GLI2 in chondrocyte proliferation has been demonstrated in vitro (61) and in vivo (62) models. Notably, skeletal anomalies in *Ihh*$^{-/-}$ embryos were completely reversed by the exogenous expression of constitutively active GLI2 in the *Ihh*$^{-/-}$; *Gli3*$^{-/-}$ background (63). In the present study, the ectopic expression of a phosphomimetic mutant (GLI2^{S252E}) promoted the proliferation of *Dyrk2*$^{-/-}$ primary cells, at least in vitro (Fig. 5 *I–K*). These data suggest that the DYRK2-mediated phosphorylation of GLI2^{S252} contributes to tissue development by fostering the proliferation and aggregation of cartilage progenitor cells. However, given the multistage development of the limb, further in vivo studies in transgenic animals are required to confirm the function of DYRK2 via the phosphorylation of GLI2 and to determine whether the exogenous expression of GLI2^{S252} or DYRK2 ameliorates the symptoms of malformations caused by abnormal Hh signaling.

From another perspective, despite the expression of *Dyrk2* in the neural tube as well as limb buds (*SI Appendix,* Fig. S12), abnormalities are not generally observed in the neural tube of *Dyrk2*$^{-/-}$ mice (28). Among the CMGC kinase family, *Ccrk*$^{-/-}$ mice exhibit developmental defects in both the neural tube and limb (30). On the other hand, *Cilk1*$^{-/-}$ mice also show abnormalities in limb formation but not neural tube patterning (29). It is therefore possible that other unidentified molecules tissue-selectively compensate for the functions of DYRK2 and CILK1 in the neural tube. Alternatively, variations in SMO-independent ANKMY2-adenylyl cyclase signaling (64) or in the length of primary cilia (65) among different cell types may influence the activation level of the Hh signaling pathway. Identifying these compensatory molecules or regulatory mechanisms unique to each cell type will lead to an understanding of the tissue-specific regulation of cilium-generated signaling including Hh signaling.

Materials and Methods

The information of plasmid constructs, animal care, animals, cell culture and transfection, generation of Dox-inducible DYRK2-BioID2-expressing cell lines, siRNA knockdown, RNA-seq, RT-qPCR, immunocytochemistry, pull-down of biotinylated proteins, proximity labeling coupled with affinity purification and mass spectrometry, STRING, KEGG, and reactome pathway analysis, IB, cell fractionation, IP, in vitro kinase assay, lentiviral preparation and infection, quantification of the ratio of nuclear to cytoplasmic fluorescence, peptides, antibody generation, SPR analysis, immunohistochemistry, DIG-in situ hybridization, in situ HCR, Alcian Blue and Alizarin Red double staining, HE, Alcian Blue, and von Kossa staining, primary cell culture and differentiation assay, CRISPR/Cas9-mediated knockout experiments, and statistical analysis are in *SI Appendix*.

Data, Materials, and Software Availability. Raw data of proteomics and RNA-seq data have been deposited in Japan ProteOme Standard Repository (ID: JPST002229) (66) and Gene Expression Omnibus (ID: GSE267749) (67), respectively. All other data are included in the manuscript and/or *SI Appendix*.

ACKNOWLEDGMENTS. We would like to thank Chikako Miura and Hikaru Hashida for technical assistance and Naoko Tago for technical support of the BioID system. We would also like to thank Dr. Hiroki Ueharu at the University of Michigan Medical School for constructive suggestions. We would also like to thank Dr. Helena Akiko Popiel for the English language editing. This work was partially supported by JSPS KAKENHI (grant numbers 21K06192 to S.Y. and 17H03584, 18K19484, 20H03519, and 23K18244 to K. Yoshida) and grants from the Jikei University Research Fund (to S.Y. and K. Yoshida), the Takeda Science Foundation (to S.Y.), Yamaguchi Endocrine Research Foundation (to S.Y.), the Nakatani Foundation (to S.N.), and the Uehara Memorial Foundation (to S.Y. and K. Yoshida).

Author affiliations: [a]Department of Biochemistry, The Jikei University School of Medicine, Tokyo 105-8461, Japan; [b]Radioisotope Research Facilities, The Jikei University School of Medicine, Tokyo 105-8461, Japan; [c]Center for Stable Isotope Medical Research, The Jikei University School of Medicine, Tokyo 105-8461, Japan; [d]Department of Laboratory Medicine, The Jikei University School of Medicine, Tokyo 105-8461, Japan; [e]Department of Bacteriology, The Jikei University School of Medicine, Tokyo 105-8461, Japan; [f]Center for Biofilm Science and Technology, The Jikei University School of Medicine, Tokyo 105-8461, Japan; [g]Laboratory of Amyloid Regulation, The Jikei University School of Medicine, Tokyo 105-8461, Japan; [h]Department of Molecular Biology, The Jikei University School of Medicine, Tokyo 105-8461, Japan; [i]Department of Physiological Chemistry, Graduate School of Pharmaceutical Sciences, Kyoto University, Sakyo-ku, Kyoto 606-8501, Japan; [j]Department of Biomolecular Science, Toho University, Chiba 274-8510, Japan; and [k]Department of Anatomy, Faculty of Medicine, Toho University, Tokyo 143-8540, Japan

Author contributions: S.Y. and K. Yoshida designed research; S.Y., A.K., K.A., P.W., S.S., J.T., A.T., T.T., Y.T., K. Yamada, and S.N. performed research; S.Y., A.K., K.A., P.W., S.S., A.T., Y.I., Y.K., T.T., Y.T., K. Yamada, S.N., and K.N. contributed new reagents/analytic tools; S.Y., A.K., K.A., P.W., S.S., J.T., A.T., T.T., Y.T., K. Yamada, S.N., and K. Yoshida analyzed data; and S.Y. and K. Yoshida wrote the paper.

1. P. W. Ingham, A. P. McMahon, Hedgehog signaling in animal development: Paradigms and principles. *Genes Dev.* **15**, 3059–3087 (2001).
2. L. V. Goodrich, L. Milenković, K. M. Higgins, M. P. Scott, Altered neural cell fates and medulloblastoma in mouse patched mutants. *Science* **277**, 1109–1113 (1997).
3. X. M. Zhang, M. Ramalho-Santos, A. P. McMahon, Smoothened mutants reveal redundant roles for Shh and Ihh signaling including regulation of L/R symmetry by the mouse node. *Cell* **106**, 781–792 (2001).
4. B. St-Jacques, M. Hammerschmidt, A. P. McMahon, Indian hedgehog signaling regulates proliferation and differentiation of chondrocytes and is essential for bone formation. *Genes Dev.* **13**, 2072–2086 (1999).
5. P. Niewiadomski, R. Rohatgi, Measuring expression levels of endogenous Gli genes by immunoblotting and real-time PCR. *Methods Mol. Biol.* **1322**, 81–92 (2015).
6. R. Mo *et al.*, Specific and redundant functions of Gli2 and Gli3 zinc finger genes in skeletal patterning and development. *Development* **124**, 113–123 (1997).
7. C. C. Hui, S. Angers, Gli proteins in development and disease. *Annu. Rev. Cell Dev. Biol.* **27**, 513–537 (2011).
8. D. Huangfu *et al.*, Hedgehog signalling in the mouse requires intraflagellar transport proteins. *Nature* **426**, 83–87 (2003).
9. T. Eguether *et al.*, IFT27 links the BBSome to IFT for maintenance of the ciliary signaling compartment. *Dev. Cell* **31**, 279–290 (2014).
10. C. J. Haycraft *et al.*, Gli2 and Gli3 localize to cilia and require the intraflagellar transport protein polaris for processing and function. *PLoS Genet.* **1**, e53 (2005).
11. J. F. Reiter, M. R. Leroux, Genes and molecular pathways underpinning ciliopathies. *Nat. Rev. Mol. Cell Biol.* **18**, 533–547 (2017).
12. P. Niewiadomski *et al.*, Gli proteins: Regulation in development and cancer. *Cells* **8**, 147 (2019).
13. T. Scheidt *et al.*, Phosphoproteomics of short-term hedgehog signaling in human medulloblastoma cells. *Cell Commun. Signal.* **18**, 99 (2020).
14. M. Tuson, M. He, K. V. Anderson, Protein kinase A acts at the basal body of the primary cilium to prevent Gli2 activation and ventralization of the mouse neural tube. *Development* **138**, 4921–4930 (2011).
15. S. Mukhopadhyay *et al.*, The ciliary G-protein-coupled receptor Gpr161 negatively regulates the Sonic hedgehog pathway via cAMP signaling. *Cell* **152**, 210–223 (2013).
16. B. Wang, J. F. Fallon, P. A. Beachy, Hedgehog-regulated processing of Gli3 produces an anterior/posterior repressor gradient in the developing vertebrate limb. *Cell* **100**, 423–434 (2000).

17. E. W. Humke, K. V. Dorn, L. Milenkovic, M. P. Scott, R. Rohatgi, The output of Hedgehog signaling is controlled by the dynamic association between suppressor of fused and the Gli proteins. *Genes Dev.* **24**, 670–682 (2010).
18. P. Niewiadomski *et al.*, Gli protein activity is controlled by multisite phosphorylation in vertebrate Hedgehog signaling. *Cell Rep.* **6**, 168–181 (2014).
19. D. Tempé, M. Casas, S. Karaz, M. F. Blanchet-Tournier, J. P. Concordet, Multisite protein kinase A and glycogen synthase kinase 3beta phosphorylation leads to Gli3 ubiquitination by SCFbetaTrCP. *Mol. Cell. Biol.* **26**, 4316–4326 (2006).
20. A. F. Cooper *et al.*, Cardiac and CNS defects in a mouse with targeted disruption of suppressor of fused. *Development* **132**, 4407–4417 (2005).
21. M. H. Chen *et al.*, Cilium-independent regulation of Gli protein function by Sufu in Hedgehog signaling is evolutionarily conserved. *Genes Dev.* **23**, 1910–1928 (2009).
22. C. Wang, Y. Pan, B. Wang, Suppressor of fused and Spop regulate the stability, processing and function of Gli2 and Gli3 full-length activators but not their repressors. *Development* **137**, 2001–2009 (2010).
23. J. Svärd *et al.*, Genetic elimination of suppressor of fused reveals an essential repressor function in the mammalian Hedgehog signaling pathway. *Dev. Cell* **10**, 187–197 (2006).
24. R. Rohatgi, L. Milenkovic, M. P. Scott, Patched1 regulates hedgehog signaling at the primary cilium. *Science* **317**, 372–376 (2007).
25. H. Tukachinsky, L. V. Lopez, A. Salic, A mechanism for vertebrate Hedgehog signaling: Recruitment to cilia and dissociation of SuFu-Gli protein complexes. *J. Cell Biol.* **191**, 415–428 (2010).
26. N. F. Wilson, J. K. Iyer, J. A. Buchheim, W. Meek, Regulation of flagellar length in Chlamydomonas. *Semin. Cell Dev. Biol.* **19**, 494–501 (2008).
27. L. W. Tam, P. T. Ranum, P. A. Lefebvre, CDKL5 regulates flagellar length and localizes to the base of the flagella in Chlamydomonas. *Mol. Biol. Cell* **24**, 588–600 (2013).
28. S. Yoshida *et al.*, The novel ciliogenesis regulator DYRK2 governs Hedgehog signaling during mouse embryogenesis. *Elife* **9**, e57381 (2020).
29. H. Moon *et al.*, Intestinal cell kinase, a protein associated with endocrine-cerebro-osteodysplasia syndrome, is a key regulator of cilia length and Hedgehog signaling. *Proc. Natl. Acad. Sci. U.S.A.* **111**, 8541–8546 (2014).
30. A. Snouffer *et al.*, Cell cycle-related kinase (CCRK) regulates ciliogenesis and Hedgehog signaling in mice. *PLoS Genet.* **13**, e1006912 (2017).
31. T. Chaya, Y. Omori, R. Kuwahara, T. Furukawa, ICK is essential for cell type-specific ciliogenesis and the regulation of ciliary transport. *EMBO J.* **33**, 1227–1242 (2014).
32. Y. Omori *et al.*, Negative regulation of ciliary length by ciliary male germ cell-associated kinase (Mak) is required for retinal photoreceptor survival. *Proc. Natl. Acad. Sci. U.S.A.* **107**, 22671–22676 (2010).
33. I. T. Wang *et al.*, Loss of CDKL5 disrupts kinome profile and event-related potentials leading to autistic-like phenotypes in mice. *Proc. Natl. Acad. Sci. U.S.A.* **109**, 21516–21521 (2012).
34. K. Nakamura *et al.*, Anterograde trafficking of ciliary MAP kinase-like ICK/CILK1 by the intraflagellar transport machinery is required for intraciliary retrograde protein trafficking. *J. Biol. Chem.* **295**, 13363–13376 (2020).
35. T. Noguchi, K. Nakamura, Y. Satoda, Y. Katoh, K. Nakayama, CCRK/CDK20 regulates ciliary retrograde protein trafficking via interacting with BROMI/TBC1D32. *PLoS One* **16**, e0258497 (2021).
36. R. M. Sears, D. G. May, K. J. Roux, BioID as a tool for protein-proximity labeling in living cells. *Methods Mol. Biol.* **2012**, 299–313 (2019).
37. K. Yamada *et al.*, Extended-synaptotagmin 1 engages in unconventional protein secretion mediated via SEC22B(+) vesicle pathway in liver cancer. *Proc. Natl. Acad. Sci. U.S.A.* **119**, e2202730119 (2022).
38. S. Maddika, J. Chen, Protein kinase DYRK2 is a scaffold that facilitates assembly of an E3 ligase. *Nat. Cell Biol.* **11**, 409–419 (2009).
39. R. Morrugares *et al.*, Phosphorylation-dependent regulation of the NOTCH1 intracellular domain by dual-specificity tyrosine-regulated kinase 2. *Cell. Mol. Life Sci.* **77**, 2621–2639 (2020).
40. N. Taira *et al.*, DYRK2 priming phosphorylation of c-Jun and c-Myc modulates cell cycle progression in human cancer cells. *J. Clin. Invest.* **122**, 859–872 (2012).
41. M. Varjosalo *et al.*, Application of active and kinase-deficient kinome collection for identification of kinases regulating hedgehog signaling. *Cell* **133**, 537–548 (2008).
42. L. E. Campbell, C. G. Proud, Differing substrate specificities of members of the DYRK family of arginine-directed protein kinases. *FEBS Lett.* **510**, 31–36 (2002).
43. S. Himpel *et al.*, Specificity determinants of substrate recognition by the protein kinase DYRK1A. *J. Biol. Chem.* **275**, 2431–2438 (2000).
44. R. Singh, M. Lauth, Emerging roles of DYRK kinases in embryogenesis and hedgehog pathway control. *J. Dev. Biol.* **5**, 13 (2017).
45. X. Wen *et al.*, Kinetics of hedgehog-dependent full-length Gli3 accumulation in primary cilia and subsequent degradation. *Mol. Cell. Biol.* **30**, 1910–1922 (2010).
46. J. Kim, M. Kato, P. A. Beachy, Gli2 trafficking links Hedgehog-dependent activation of Smoothened in the primary cilium to transcriptional activation in the nucleus. *Proc. Natl. Acad. Sci. U.S.A.* **106**, 21666–21671 (2009).
47. A. L. Cherry *et al.*, Structural basis of SUFU-GLI interaction in human Hedgehog signalling regulation. *Acta Crystallogr. D Biol. Crystallogr.* **69**, 2563–2579 (2013).
48. Y. Zhang *et al.*, Structural insight into the mutual recognition and regulation between suppressor of fused and Gli/Ci. *Nat. Commun.* **4**, 2608 (2013).
49. Y. Tsuneoka, H. Funato, Modified in situ hybridization chain reaction using short hairpin DNAs. *Front. Mol. Neurosci.* **13**, 75 (2020).
50. Y. Katayama *et al.*, Seawater transfer down-regulates C-type natriuretic peptide-3 expression in prolactin-producing cells of Japanese eel: Negative correlation with plasma chloride concentration. *Mol. Cell. Endocrinol.* **507**, 110780 (2020).
51. M. K. S. Wong, Y. Tsuneoka, T. Tsukada, Subcellular localization of Na(+)/K(+)-ATPase isoforms resolved by in situ hybridization chain reaction in the gill of chum salmon at freshwater and seawater *Fish Physiol. Biochem.* **49**, 751–767 (2023).
52. P. Aghajanian, S. Mohan, The art of building bone: Emerging role of chondrocyte-to-osteoblast transdifferentiation in endochondral ossification. *Bone Res.* **6**, 19 (2018).
53. S. Egawa, S. Miura, H. Yokoyama, T. Endo, K. Tamura, Growth and differentiation of a long bone in limb development, repair and regeneration. *Dev. Growth Differ.* **56**, 410–424 (2014).
54. Y. Han *et al.*, Phosphorylation of Ci/Gli by fused family kinases promotes hedgehog signaling. *Dev. Cell* **50**, 610–626.e4 (2019).
55. B. Baran, K. Kosieradzka, W. Skarzynska, P. Niewiadomski, MRCKα/β positively regulates Gli protein activity. *Cell Signal.* **107**, 110666 (2023).
56. B. Zhang *et al.*, GSK3β-Dzip1-Rab8 cascade regulates ciliogenesis after mitosis. *PLoS Biol.* **13**, e1002129 (2015).
57. K. H. Lee *et al.*, Identification of a novel Wnt5a-CK1ε-Dvl2-Plk1-mediated primary cilia disassembly pathway. *EMBO J.* **31**, 3104–3117 (2012).
58. S. J. Matissek, S. F. Elsawa, GLI3: A mediator of genetic diseases, development and cancer. *Cell Commun. Signal.* **18**, 54 (2020).
59. A. J. Bardwell *et al.*, ERK2 MAP kinase regulates SUFU binding by multisite phosphorylation of GLI1. *Life Sci Alliance* **5**, e202101353 (2022).
60. S. Ohba, Hedgehog signaling in skeletal development: Roles of Indian hedgehog and the mode of its action. *Int. J. Mol. Sci.* **21**, 6665 (2020).
61. F. Long, X. M. Zhang, S. Karp, Y. Yang, A. P. McMahon, Genetic manipulation of hedgehog signaling in the endochondral skeleton reveals a direct role in the regulation of chondrocyte proliferation. *Development* **128**, 5099–5108 (2001).
62. B. Yan *et al.*, mTORC1 regulates PTHrP to coordinate chondrocyte growth, proliferation and differentiation. *Nat. Commun.* **7**, 11151 (2016).
63. K. S. Joeng, F. Long, The Gli2 transcriptional activator is a crucial effector for Ihh signaling in osteoblast development and cartilage vascularization. *Development* **136**, 4177–4185 (2009).
64. B. N. Somatilaka *et al.*, Ankmy2 prevents smoothened-independent hyperactivation of the Hedgehog pathway via cilia-regulated adenylyl cyclase signaling. *Dev. Cell* **54**, 710–726 (2020).
65. V. Macarelli, E. Leventea, F. T. Merkle, Regulation of the length of neuronal primary cilia and its potential effects on signalling. *Trends Cell Biol.* **33**, 979–990 (2023).
66. S. Nagamori, Interactome of DYRK2 by using BioID proximity labeling. Japan ProteOme Standard Repository. https://repository.jpostdb.org/. Deposited 1 July 2023.
67. S. Yoshida *et al.*, Positive regulation of Hedgehog signaling via phosphorylation of GLI2/GLI3 by DYRK2 kinase. Gene Expression Omnibus at NCBI. https://www.ncbi.nlm.nih.gov/geo/. Deposited 17 May 2024.